ISSN 0915-633X

NATIONAL INSTITUTE FOR FUSION SCIENCE

Design of Modular Coils for a Quasi-axisymmetric Stellarator with a Flexible Control of the Magnetic Field Configuration

A. Shimizu, S. Okamura, M. Isobe, C. Suzuki,
S. Nishimura, T. Watari, K. Matsuoka

(Received - July 29, 2002)

NIFS-737 Aug. 2002

RESEARCH REPORT
NIFS Series

TOKI, JAPAN

Design of modular coils for a quasi-axisymmetric stellarator with a flexible control of the magnetic field configuration

A. Shimizu, S. Okamura, M. Isobe, C. Suzuki, S. Nishimura, T. Watari, K. Matsuoka

National Institute for Fusion Science, Toki 509-5292, Japan

Abstract

A design of the modular coil system for CHS-qa has been made for the plasma configuration "2b32" with the aspect ratio 3.2. The magnetic field strength and the major radius are 1.5 T and 1.5 m, respectively. The normal component of magnetic field produced by the modular coils is minimized on the plasma boundary to obtain the optimum coil design. We put engineering constraint on the distance between adjacent modular coils and the radius of coil curvature. The dependence of the residual normal component of the field on these conditions is examined, and the realistic values for them are selected. Additional coils to control various properties of the magnetic field configuration (the rotational transform, the magnetic well depth, *etc.*) have been designed and a flexibility of the magnetic field configuration is realized. For the case that the rotational transform crosses the low-order rational value resulting in magnetic islands, the residues of islands are evaluated with which a further improvement of coil design can be made to eliminate magnetic islands.

Keywords quasi-axisymmetric stellarator, modular coil system, engineering design, poloidal coil, CHS-qa

1. Introduction

A helical system has a three-dimensional magnetic field configuration, and this nature offers significantly large freedom of choice in designing a plasma confinement configuration. Recently, advanced stellarator configurations, which have better properties in the neoclassical transport and MHD stability, have been developed [1-4]. A tokamak has an axisymmetric magnetic field, in which an invariance of the canonical momentum exists and the excursion of particle orbit from the magnetic surface is limited. It was shown that, in a Boozer magnetic coordinate system [5], the guiding center orbit of particle is determined only by the $|\mathbf{B}|$ structure. A quasi-axisymmetric configuration [6,7] has the axially symmetric magnetic field in this coordinate system, therefore a tokamak-like neoclassical transport property can be expected. Since helical systems need no inductive current, a quasi-axisymmetric stellarator has essentially no problem for a steady-state operation. Another advantage is that it is much easier to design a low aspect ratio configuration compared to conventional stellarators, which is a common characteristic of advanced stellarators. Therefore this configuration has an attractive feature for a compact-sized steady state reactor.

CHS-qa [8,9] is a quasi-axisymmetric device with a low aspect ratio of 3.2 (the major radius of 1.5 m / the minor radius of 0.47 m), and its design work has been continued at National Institute for Fusion Science (NIFS). The strength of the magnetic field is

designed to be 1.5 T. In a design process of recent advanced stellarators, a magnetic field configuration is determined based on the boundary structure in the first step without considering the coil geometry [10]. For the second step, the modular coil shape is designed to realize this configuration in an actual device [11]. Continuous windings of helical coils have been used as a conventional way of designing helical devices [12]. It is possible to produce a quasi-axisymmetric configuration with continuous helical winding coils, however, winding lows become complicated and very difficult to construct. For this reason, continuous helical coils are not suitable to create the designed magnetic field of quasi-axisymmetric configuration, and designing modular coil system is needed. The modular coils are required not only to produce the quasi-axisymmetric configuration with a good accuracy, but also to have moderate shapes from the engineering point of view. However, these two requirements are generally contradictory, and we must make a compromise to determine the realistic coil geometry. In this paper, we present the design work of modular coils for CHS-qa.

The modular coil system of CHS-qa, in principle, does not need additional poloidal coils. This is different from conventional helical systems and tokamaks (It is possible to design a conventional helical system with no poloidal coils, however this configuration is not suitable to a real experimental machine). However, the flexibility of field configuration is important for plasma experiments so that we could investigate effectively various physics issues related to the quasi-axisymmetric concept. To study an effect of non-axisymmetric components on the neoclassical transport, it is desirable to change some of non-axisymmetric components can be varied. The rotational transform is an important parameter for MHD stability. It is possible to vary it by using auxiliary toroidal field coils. The poloidal coils provide several flexibilities of the configuration (magnetic well depth, shear and quasi-axisymmetry) through the shaping of the plasma cross section. We discuss about these flexibilities of CHS-qa magnetic field configuration achieved by its coil system.

2. Modular coil design

Equilibrium properties of a toroidal configuration are determined by the shape of the outermost magnetic surface [13]. The VMEC code is the most popular tool to solve the three dimensional equilibrium problem [14]. In this code, the shape of the plasma boundary is parameterized with a relatively small number of parameters: a set of coefficients of Fourier series. By using this small number of parameters this code can calculate the equilibrium, if the pressure profile and the plasma current profile are given.

For the computational design of an advanced stellarator configuration, the shape of outermost plasma boundary is optimized so that the configuration has good properties in MHD stability, the neoclassical transport, *etc.* The configuration of a present candidate for CHS-qa configuration (we call this as "2b32") has better neoclassical transport property that is realized by introducing the quasi-axisymmetry. The MHD properties of interchange and ballooning modes are also improved by including evaluation of these properties in the process of configuration optimization. Details of optimization process and physical properties of this configuration was shown in the paper [15].

In order to realize the magnetic field configuration in a real device, modular coils must

be designed based on the outermost plasma boundary data obtained by the configuration optimization described above (we call this boundary as a plasma boundary). If we make $\mathbf{B} \cdot \mathbf{n}$ zero on the plasma boundary, all properties of magnetic field configuration are determined by the Neumann boundary condition. (Here $\mathbf{B}$ is vacuum magnetic field produced by modular coils on the plasma boundary and $\mathbf{n}$ is the normal unit vector of this surface.) Therefore, it is sufficient to take into account only the condition that $\mathbf{B} \cdot \mathbf{n}$ equals zero at the outermost plasma boundary. This process to determine the modular coil geometry is done by the NESCOIL code [16]. In this code, modular coils are expressed by the coefficients of Fourier series. Detail of expression for modular coils are shown in appendix. Favorable values for these coefficients are searched to satisfy the Neumann boundary condition.

All modular coils are located between two limiting toroidal surfaces. As a starting point of modular coil design, we give the shapes of limiting surfaces with Fourier coefficients. Considering the size of vacuum chamber, the position of inner limit surface is determined. The vacuum chamber is located at about 8 cm away from the plasma boundary surface. Taking marginal distance (for the space of modular coils which have finite cross section, thickness of vacuum chamber *etc.*) into account, 26 cm is selected for the distance between plasma boundary and inner limit surface. The size of outer limit surface determines the size of a modular coil, namely it determines the magnitude of bumpy ripple produced by discrete modular coils. In order that this ripple should be blow the maximum of non-axisymmetric component at the plasma boundary, the position of the outer limit surface is located at 45 cm away from the plasma boundary.

In Fig.1, the modular coils of CHS-qa obtained by this coil optimization procedure are shown. The plasma configuration, "2b32" version, is a present candidate for the CHS-qa device which has an aspect ratio of 3.2 [15]. The total number of modular coils is 20, which is selected with the consideration of magnitude of bumpy ripple created by discrete coils. The criterion of this ripple is 2.0 % of magnetic field strength at the plasma boundary, which is below the maximum of non-axisymmetric components. If the total number is increased, this ripple can be reduced but cost for machine construction becomes more expensive. Accessibility to plasma is also deteriorated. If decreased, bumpy ripple increases and cannot be suppressed to the criterion level on the condition of realistic coil curvature. Because N is 2 and the configuration has the stellarator symmetry, the whole torus consists of four identical parts. Therefore modular coils have five different shapes. The solution of the NESCOIL code gives only a shape of coil filaments. Modular coils in Fig.1 have finite sized cross-sections, which are determined so that the centers of cross-sections fit with these coil filaments. The coil cross section is rectangular, of which area is 21 cm x 16 cm including normal copper conductors, insulation and the coil casing.

The maximum magnetic field strength (1.5 T) and the pulse length (1 sec) of keeping up this field strength require 13.1 cm x 8.2 cm squared area of cross section for conductor and water cooling. Cross section of a conductor wire is 0.82 cm x 0.82 cm rectangular and it has a circular channel for water-cooling at the center, of which diameter is 0.4 cm. One modular coil consists of 160 (16 x 10) turns of this wire. The large electromagnetic force acts on a modular coil in the duration of discharge and the copper conductor is not endurable. To support the conductor, the thickness of 3 cm stainless steel coil-casing covers it. The thickness of coil-casing is determined based on the calculation results of

electromagnetic forces acting on the conductor. Taking the thickness of 1cm insulation between coil casing and conductor into account, the cross section of modular coils becomes 21 cm x 16 cm.

In Fig.2, the magnetic surfaces (Poincare plots) are shown, which are obtained by tracing magnetic field produced by these modular coils. In this calculation, the coil is assumed to be a filament. The calculation with finite size of current distribution does not cause significant change in results. Cross sections at the toroidal angle of $\varphi = 0°, 45°, 90°$ are shown ($\varphi = 0°$ corresponds to the position of the vertically elongated cross section). In these figures, plasma boundary (solid line) is also shown. The average of $\mathbf{B} \cdot \mathbf{n} / |\mathbf{B}|$ (the normal component of produced magnetic field at the plasma boundary normalized by the magnetic field strength.) is below 1.4 %. Maximum value is about 4 %. The average value cannot be reduced below this level on the condition of 20 for total number of coils that have realistic curvature. The rotational transform and the magnetic well depth obtained from these modular coils are compared with the result of VMEC calculation in Fig.3. In this figure, ρ means the normalized average minor radius. This figure shows that the radial profiles of these quantities produced by the modular coils agree well with the profiles given by the VMEC calculation. This is reasonable because Fig.2 shows a good agreement in the shapes of the magnetic surface boundary and the VMEC plasma boundary.

To evaluate the quasi-axisymmetry of the magnetic field configuration, Fourier spectra of the magnetic field strength in the Boozer coordinate are used ($|\mathbf{B}| = \Sigma B_{mn} \cos(m\theta - nN\phi)$). The spectra of the "2b32" magnetic configuration in Boozer coordinate obtained from VMEC equilibrium are shown in Fig.4a. In this figure, amplitudes of spectra are calculated for the magnetic field strength of 1.5 T. The dominant term is B_{10}, which arises from the toroidal effect. In Fig.4b, B_{mn}s of the magnetic field produced by the modular coils are shown. The B_{mn}s in this figure are in a good agreement with B_{mn}s in Fig.4a (VMEC results) except for B_{01}. The reason of the disagreement in B_{01} is that the change of this mirror ripple does not affect the normal component of produced magnetic field at the plasma boundary largely. Therefore, it is difficult to realize the designed value of this ripple component only by reducing $\mathbf{B} \cdot \mathbf{n} / |\mathbf{B}|$ at the plasma boundary. (This fact implies that we can control the mirror ripple without a significant change of magnetic surface geometry. The control scheme of this ripple is discussed in section 3.) In order to realize the designed value of mirror ripple, B_{01}, the evaluation of this ripple was included in the coil optimization process. The B_{mn} after this optimization process are shown in Fig.4c. By including the evaluation of B_{01} in the code, we can make the value of B_{01} close to zero at the magnetic axis successfully and can also realize designed values of other B_{mn}s. In Fig4d, the calculation result of neoclassical diffusion coefficient by using the expression of Beidler and Hitchon [17] is shown. The curve (a) is the diffusion coefficient of configuration obtained from VMEC (B_{mn} in Fig.4a). The curve (b) is the diffusion coefficient of configuration obtained from modular coil system, however in which optimization the B_{01} evaluation is not included (B_{mn} in Fig.4b). The curve (c) is the diffusion coefficient obtained from modular coil system, in which optimization B_{01} evaluation is included (B_{mn} in Fig.4c). The experimental range of normalized collision frequency ν^* is 0.01 ~ 0.1. In this range, the diffusion coefficient of non-B_{01} optimization case is larger than that of designed configuration that is calculated by VMEC. At ν^* =

0.008 the diffusion coefficient of non-B_{01} optimization case is twice as large as designed configuration and this deterioration is not negligible. By including the evaluation of B_{01} in coil optimization, the diffusion coefficient is decreased to 0.058 (curve c) at $\nu^* = 0.008$, which is smaller compared with 0.083 (curve a) of designed configuration. The purpose of the B_{01} evaluation is the realization of same or below of the designed configuration's value in the diffusion coefficient, and the optimization of B_{01} is sufficient. The profiles of rotational transform and magnetic well depth are not changed so much by this inclusion. They are reproduced well by the improved modular coil system, which is the same as the case of non-ripple-optimized coil system.

From the engineering point of view, the distance between adjacent coils and the radius of coil curvature are important parameters. If the curvature is too tight, it is difficult to wind the conductor. If the distance is too small, the spaces for the supporting structures (also for diagnostic ports) are not enough and in the worst case the coils can not be assembled physically. On the contrary, if the small radius of curvature and the small distance between coils are accepted in the coil design, it becomes much easier to reduce the normal component of produced magnetic field at the plasma boundary ($\mathbf{B} \cdot \mathbf{n} / |\mathbf{B}|$).

We investigate how $\mathbf{B} \cdot \mathbf{n} / |\mathbf{B}|$ depends on the condition of the minimum radius of curvature of coils and distance between adjacent coils. To do this, we make a number of separate optimization designs with different conditions of the radius of curvature and the distance between coils. In this study, we apply these conditions on the coil filament. In Fig.5a, $\mathbf{B} \cdot \mathbf{n} / |\mathbf{B}|$ (average and maximum values) is shown as a function of minimum radius of curvature. In this case, the minimum distance between adjacent coils is fixed to be 22 cm. The maximum value of $\mathbf{B} \cdot \mathbf{n} / |\mathbf{B}|$ depends on the condition of the minimum radius of curvature although the average $\mathbf{B} \cdot \mathbf{n} / |\mathbf{B}|$ does not depend on it. The improvement of the reduction of $\mathbf{B} \cdot \mathbf{n} / |\mathbf{B}|$ by decreasing the condition of minimum radius of curvature becomes smaller near 25 cm as shown in Fig.5a. The minimum-limit for this value is actually determined from the engineering point of view. For the wire can be windable, the value of minimum radius of curvature must be larger than 10 times of a side of square wire, namely than 8 cm. We select 11 cm for this value in order to include safety factor. In this case, the minimum radius of curvature for filament coil becomes 25 cm. Therefore the value of 25 cm is the allowable level, and we select this reasonable value to reduce the normal component of magnetic field.

On the other hand, in Fig.5b, $\mathbf{B} \cdot \mathbf{n} / |\mathbf{B}|$ is shown as a function of the minimum distance between adjacent coils by keeping the minimum radius of curvature at 26 cm. The dependence of $\mathbf{B} \cdot \mathbf{n} / |\mathbf{B}|$ (average and maximum) on the condition of minimum distance becomes weaker near the condition of 22 cm. Taking account of the size of coil cross section, the distance between modular coil must be above 21 cm. Therefore we select 22 cm as the minimum distance between adjacent coils.

Finally, the conditions imposed in the coil design for Fig.1 are the minimum radius of curvature of 25 cm and the minimum distance between adjacent coils of 22 cm. These values are for coil filaments. In Fig.6, the radius of curvature of the modular coils, which have a finite-sized cross-section, is shown as colors. In this figure, 5 types of modular coils are numbered in the order of the toroidal angle (these numbers correspond with ones shown in Fig.1). The position of coil 1 is close to the vertically elongated cross section (φ = 0°, 180°) and coil 5 is to the horizontally elongated one (φ = 90°, 270°). Among 5

types of coils, coils closer to the horizontally elongated cross section have a smaller radius of curvature. The radius of curvature in this figure is evaluated on the surface of coil structure (not for the coil filaments). The minimum radius of curvature becomes 11 cm at the corner of the rectangular cross section, although it is 25 cm for the coil filament. The minimum distance between finite-sized coils becomes nearly 0 cm at the inboard side of the vertically elongated cross section ($\varphi = 0°$, 180°).

3. The flexibility of magnetic field configuration

In order to make the experiment productive, it is required for the experimental device to have knobs to modify properties of the magnetic field configuration (such as the rotational transform, the magnetic shear, residual ripples *etc.*). In CHS-qa, three methods are planned for modifications of magnetic field configuration: 3 pairs of poloidal coils, the auxiliary toroidal field coils and a control of current ratio in the main modular coils.

Three pairs of poloidal coils are of the same type as in CHS and LHD. The positions of these circular coils are shown schematically in Fig.7. Careful selections of positions of these poloidal coils enable the following modes of operation: one operation that creates combination of the vertical and quadrupole fields with different ratios, and another operation that varies the magnetic flux in the torus center keeping the vertical field unchanged. Since the standard magnetic configuration is produced by modular coil, the current of poloidal coils is needed only when magnetic configuration is changed. Therefore no larger current is required for poloidal coils than in the CHS heliotron/torsatron, since the standard configuration of CHS requires the large poloidal coil current same order to helical coil current.

Applying the additional vertical fields is an effective way of varying physical characteristics of magnetic field configuration of CHS-qa. The position of the magnetic axis is shifted by the vertical field. Figure 8a and 8b show Poincare plots of the inward and the outward axis shifted cases, respectively. The amount of vertical field in each case is 1 % of the main magnetic field strength. It is general characteristics that there is a point at the outboard side of confinement region, beyond which closed magnetic surfaces never expand. In our case, the position of this point on a poloidal cross section of $\varphi = 0$ is at R = 2.03 m on the Z = 0 m plane. Since this point determines the volume of outermost magnetic surface, the volume in the outward shift case is decreased. The shift of the magnetic axis has an effect on the rotational transform, because the strength of toroidal magnetic field is changed. Figure 9 shows the radial profiles of the rotational transform for both inward and outward shift cases with the standard case as a reference. By the inward shift of the magnetic axis, we can decrease the rotational transform, and vice versa. The magnetic well depth is also changed by the magnetic axis shift. In the case of inward shift, the well depth becomes deeper. In these two cases of the axis shift control, the amount of residual ripples also changes. In Fig.10a and b, the spectra of magnetic field strength in Boozer's coordinates in each case are shown. In the case of inward shift, residual ripples, such as $B_{0,1}$ and $B_{1,1}$, increase and the quasi-axisymmetry is degraded. However, in the case of outward shift, the quasi-axisymmetry becomes better. This is because that the non-axisymmetric component B_{01} is reduced by the outward shift of magnetic axis. Another reason is that the change of volume by outward shift reduces the

region where non-axisymmetric component is large. The good quasi-axisymmetry of outward shift configuration leads to the improvement of neoclassical transport property. The diffusion coefficient (D) of this configuration as a function of normalized collision frequency is shown in Fig 10c (curve b). The D of outward shift case is improved in 1/v regime compared with standard configuration (curve c). On the contrary, the D of inward shift case (curve a) is increased by the deterioration of quasi-axisymmetry.

The poloidal coils can produce a quadrupole field, by which the shaping of vertical or horizontal elongation is possible. Figure 11 shows magnetic surfaces when a quadrupole field is applied to CHS-qa. The amount of quadrupole field is 0.75% of the main magnetic field strength at (R,Z) = (1.5 m, 0.4 m). Figure11a and 11b show the cases of vertical and horizontal elongation, respectively. With the control of a quadrupole field, the radial profile of rotational transform can be changed as shown in Fig.12. In the horizontally elongated case, the rotational transform at the plasma center is increased. On the contrary, in the vertically elongated case, it is decreased at the center, increasing the shear (it corresponds to negative shear in tokamak) in the outer region ($\rho \geq 0.6$). The magnetic well depth also increases for the vertically elongated case. The quasi-axisymmetry changes little by these shaping controls.

To confirm the advantage of the quasi-axisymmetric configuration experimentally, we need to control the grade of quasi-axisymmetry of configuration. For this purpose, a mirror ripple component is applied to the quasi-axisymmetric configuration of CHS-qa. Two electric power supplies for CHS-qa modular coils are used; by changing the ratio of current in the main modular coils the mirror ripple can be controlled. The B_{mn}s for the modified ratio of modular coil currents are shown in Fig.13. In this case, the coil current of 8 (4 per one period. In Fig.1 and Fig.5, coil1 and coil2.) modular coils close to vertically elongated cross sections (at toroidal angle $\varphi \sim 0°$ and 180°) are reduced to 80 % of the other coils. The amount of B_{01} is increased effectively without a significant change in other non-axisymmetric components except for B_{02} (this is the second harmonics of B_{01}). In Fig.14, Poincare plot in this case is shown. The solid line shows the shape of plasma boundary, which is the same as that in Fig.2. When the mirror ripple is controlled, the change in the shape of the magnetic surface from the standard configuration is not so large. Thus, the mirror ripple can be controlled keeping the plasma volume. The profiles of the rotational transform and magnetic well in this case are shown in Fig.15. The magnetic well depth does not change. The rotational transform decreases at the center.

The mirror ripple control has two important aspects in the experimental study of CHS-qa. One is its effect on the neoclassical transport and another is on the viscosity. Due to this mirror ripple, the quasi-axisymmetry is degraded and the neoclassical diffusion loss increases. Figure 16 shows the electron diffusion coefficient when the mirror ripple is increased. For comparison, the diffusion coefficients of the 2b32 standard configuration and of the conventional helical device CHS [18] are also shown. In the evaluation of these coefficients, the magnetic field model by Beidler and Hitchon [17] was used. By the control of mirror ripple, we can increase the diffusion coefficient of CHS-qa and make it closer to that of CHS.

It is well known that the shear of the plasma rotation plays an important role to get an improved confinement, namely, the reduction of anomalous diffusion loss. To produce a large shear in the plasma rotation, the viscosity of the plasma rotation should be small.

The quasi-axisymmetric configuration has small parallel viscosity in the toroidal and poloidal directions compared with that in CHS [19], and a large plasma rotation is expected. To investigate the relation between the reduction of anomalous diffusion loss and the plasma rotation (and its shear) in a quasi-axisymmetric configuration, we need the flexibility to change the parallel viscosity of plasma. The mirror ripple component produces the bumps of magnetic field in the toroidal direction and the parallel viscosity is increased by a factor of 6 for the case of mirror ripple control described above. The detailed analysis of viscosity in a quasi-axisymmetric configuration is reported in [20].

The rotational transform is an important parameter for MHD stability and the neoclassical transport. In CHS-qa, the auxiliary toroidal field coil is installed to enhance the flexibility of the rotational transform. In Fig.17, the rotational transform is shown with the additional toroidal field. The amount of additional toroidal field is 3.2% (or -3.3%) of the main magnetic field strength. The rotational transform can be reduced (increased) uniformly in all the range of minor radius. In these cases, a significant change in the magnetic well depth does not appear. The quasi-axisymmetry does not change either.

In the control of rotational transform, its profile sometimes crosses a rational value and magnetic islands might appear at this rational surface. Magnetic islands should have bad effect on the transport, therefore the size of islands must be reduced to maintain good confinement. It is possible to eliminate these magnetic islands through the coil shape optimization. In Fig.18, an example of the elimination of the island is shown. The residue of island [21,22] is evaluated in the coil optimization process. The residue is a value that shows whether a fix point of island is o-point or x-point. If the value of residue is zero, the fix point of island becomes neither o-point nor x-point, namely the island is eliminated. By optimizing the modular coil so that the residue becomes zero, the island can be eliminated. Here we take the configuration discussed in the previous paragraph where the toroidal field is increased. The rotational transform is reduced and the profile of rotational transform crosses the rational value (1/3) at $\rho = 0.55$ and $\rho = 0.9$ (see Fig.17). Magnetic islands appear at these rational magnetic surfaces. Figure 18a shows magnetic surfaces with large islands. In the coil optimization process, we include the evaluation of the residue of these islands and reduce this value for each rational surface. Figure 18b shows magnetic surfaces obtained from the modular coils that are improved so that the residue of islands is minimized at the two rational surfaces. Magnetic islands almost disappear. The profile of rotational transform is not changed by this island reduction process.

We showed a possibility of island elimination by optimizing modular coil. This is an example of island elimination. For any other configurations, it is needed to consider several configurations having islands at the same time in optimization process. We do not know in how many other configurations we can eliminate islands at the same time. Simultaneous elimination of islands is a future issue.

4. Conclusion

The design of a modular coil system of CHS-qa has been made for the plasma configuration "2b32". It is successful to realize the magnetic field configuration that fits

to the optimized plasma configuration with a good accuracy. Engineering aspects on the manufacturing process of the real device are included by imposing constraints on the radius of coil curvature and the distance between coils. The $\mathbf{B} \cdot \mathbf{n} / |\mathbf{B}|$, the normal component of produced magnetic field at the plasma boundary, is suppressed to low level in order to obtain the good neoclassical transport property, even with realistic values for the radius of curvature and the distance.

The flexibility of magnetic field configuration is realized by three methods. 1) By using 3 pairs of poloidal coils, it is possible to change the rotational transform and the magnetic well depth. 2) The quasi-axisymmetry can be changed by controlling the current ratio of modular coils: it is possible to increase the mirror ripple component, $B_{0,1}$, without significant changes in other quantities. 3) The rotational transform can be controlled with auxiliary toroidal field coils. The control of rotational transform may result in magnetic islands appearing at the rational surface. However, by evaluating residue of islands and by optimizing the coil shape, it is possible to eliminate magnetic islands.

The rotational transform has significant effects on MHD stability and fluctuation through rational (resonant) surfaces. The control range of rotational transform shown in this paper is sufficient to avoid or create some rational surfaces. Quasi-axisymmetry can be changed so that the magnitude of neoclassical diffusion coefficient becomes close to CHS heliotron/torsatron and the helical 1/v regime becomes also accessible. Thus, the flexibility of the magnetic field configuration can be realized in CHS-qa, which is useful to study confinement physics of a quasi-axisymmetric stellarator.

Appendix

In the NESCOIL code, all modular coils are designed to lie on a single toroidal surface, which is called a current carrying surface (CCS). The shape of a modular coil on this surface is expressed as follows,

$$\eta = \alpha + \Sigma_m [a_m \cos(m\alpha) + b_m \sin(m\alpha)],$$
$$\zeta = \Sigma_m [c_m \cos(m\alpha) + d_m \sin(m\alpha)]. \quad (1)$$

Here, a_m, b_m, c_m, d_m are Fourier coefficients that are taken as variables in the code. ζ is the toroidal angle and η is the poloidal angle which is defined on CCS. The α is a parameter and the path of (η, ζ), which is made by changing α from 0 to 2π on CCS, corresponds to one modular coil filament.

CCS is also expressed by using Fourier series. The position of this surface is restricted between two limiting surfaces: the inner and outer surfaces. These limiting surfaces are expressed as follows. For the inner surface,

$$R^{(in)} = \Sigma_{mn} R^{(in)}_{mn} \cos(m\eta - nN\zeta),$$
$$Z^{(in)} = \Sigma_{mn} Z^{(in)}_{mn} \sin(m\eta - nN\zeta),$$
$$\varphi = \zeta. \quad (2)$$

For the outer surface, same form is used. Namely $R^{(in)}$, $R^{(in)}_{mn}$, $Z^{(in)}$, $Z^{(in)}_{mn}$ is replaced by $R^{(out)}$, $R^{(out)}_{mn}$, $Z^{(out)}$, $Z^{(out)}_{mn}$. Here N is a toroidal periodic number (N=2 for CHS-qa). ($R^{(in)}$, $Z^{(in)}$, φ) (and ($R^{(out)}$, $Z^{(out)}$, φ)) expresses the toroidal surface in the cylindrical coordinate. The number m and n is the Fourier mode number and the summation is taken about them. As a starting point of modular coil design, we give the shapes of limiting surfaces with Fourier coefficients, $R^{(in)}_{mn}$, $Z^{(in)}_{mn}$, $R^{(out)}_{mn}$, $Z^{(out)}_{mn}$.

By using the expression of these limiting surfaces, CCS is expressed as follows,

$$R^{(ccs)} = (1-A)\cdot R^{(in)} + A\cdot R^{(out)},$$
$$Z^{(ccs)} = (1-A)\cdot Z^{(in)} + A\cdot R^{(out)},$$
$$\varphi = \zeta. \quad (3)$$

The function $A(\eta, \zeta)$ has a value between 0 and 1, which is defined as $A=1/2\cdot(1+\tanh(F))$. Here, F is also a function of η and ζ, and this function is expressed by Fourier series, namely $F = \Sigma_{mn} F_{mn} \cos(m\eta - nN\zeta)$. The NESCOIL code takes these values F_{mn} as variables, as well as a_m, b_m, c_m, d_m, therefore the position and geometry of current carrying surface are also optimized.

Reference

[1] D. A. Spong, S. P. Hirshman, J. C. Whitson, D. B. Batchelor, B. A. Carreras, V. E. Lynch, J. A. Rome, J optimization of small aspect ratio stellarator/tokamak hybrid devices, Phys. Plasma **5** (1998) 1752-1758.

[2] J. Nührenberg, R. Zille, Stable stellataros with medium β and aspect ratio, Phys. Lett. A **114** (1986) 129-132.

[3] C. Beidler, G. Grieger, F. Herrnegger, E. Harmeyer *et al.*, Physics and Engineering Design for Wendelstein VII-X, Fusion Technology **17** (1990) 148.

[4] M. Yokoyama, Y. Nakamura, M. Wakatani, A helias-heliac hybrid stellarator, Nucl. Fusion **34** (1994) 288-294.

[5] A. H. Boozer, Guiding center drift equations, Phys. Fluids **23** (1980) 904-908.

[6] J. Nührenberg, W. Lotz, S. Gori, Quasi-axisymmetric tokamaks, Theory of Fusion Plasmas (International School of Plasma Physics, SIF, Bologna, 1994) 3-12.

[7] P. Garabedian, Stellarators with the magnetic symmetry of a tokamak, Phys. Plasmas **3** (1996) 2483-2485.

[8] K. Matsuoka, S. Okamura, M. Fujiwara, M. Drevlak, P. Merkel, J. Nuehrenberg, Post-CHS Project, Plasma Physics Reports **23** (1997) 542-546.

[9] S. Okamura, K. Matsuoka, M. Fujiwara, M. Drevlak, P. Merkel, J. Nuehrenberg, Conceptual design of a quasi-axisymmetric stellarator (CHS-qa), J. Plasma Fusion Res. SERIES **1** (1998) 164-167.

[10] J. Nührenberg, R. Zille, Quasi-helically symmetric toroidal stellarators, Phys. Lett. **A 129** (1988) 113-117.

[11] P. Merkel, Solution of stellarator boundary value problems with external currents, Nuclear Fusion **27** (1987) 867-871.

[12] K. Matsuoka, S. Kubo, M. Hosokawa, Y. Takita, S. Okamura, N. Noda, H. Yamada, H. Iguchi *et al.*, Confinement study in compact helical system (CHS), Plasma Phys. and Control. Nucl. Fusion Research **Vol.2** (1988) 411-417.

[13] F. Bauer, O. Betancourt and P. Garabedian, Magnetohydrodynamic equilibrium and stability of stellarators (Springer, NewYork, 1984).

[14] S. P. Hirshman, J. C. Whitson, Steepest-descent moment method for three-dimensional magnetohydrodynamic equilibria, Phys. Fluids **26** (1983) 3553-3568.

[15] S. Okamura, K. Matsuoka, S. Nishimura, M. Isobe, I. Nomura, C. Suzuki, A. Shimizu *et al.*, Physics and engineering design of low aspect ratio quasi-axisymmetric stellarator CHS-qa, Nuclear Fusion **41** (2001) 1865-1871.

[16] M. Drevlak, Automated optimization of stellarator coils, Fusion Technology **33** (1998) 106-117.

[17] C. D. Beidler, W. N. G. Hitchon, Ripple transport in helical-axis advanced stellarators: a comparison with classical stellarator/torsatrons, Plasma Phys. Control. Fusion **36** (1994) 317-353.

[18] S. Okamura, K. Matsuoka *et al.*, Confinement physics study in a small low aspect ratio helical device: CHS, Nuclear Fusion **39** (1999) 1337-1350.

[19] C. Suzuki, K. Ida, S. Okamura, M. Isobe, A. Shimizu, S. Nishimura, I. Nomura, K. Matsuoka, Reduction of parallel viscosity in a quasi-axisymmetric stellarator CHS-qa configuration, J. Plasma Fusion Res. SERIES **4** (2001) 457-460.

[20] C. Suzuki, K. Ida, A. Fujisawa, A. Shimizu, S. Okamura, S. Nishimura, M. Isobe, I. Nomura, K. Matsuoka, Magnetic field structure preferable to E x B shear flow generation in a quasi-axisymmetric stellarator CHS-qa, Plasma Phys. Control. Fusion **44** (2002) A225-A230.

[21] John M. Greene, Two-dimensional measure-preserving mappings, J. Math. Phys. **9** (1968) 760-768.

[22] John M. Greene, A method for determining a stochastic transition, J. Math. Phys. **20** (1979) 1183-1201.

Figure Caption

Fig.1 Modular coils of CHS-qa, top view and two side views at φ=0 degrees (vertically elongated cross section), at φ=90 degrees (horizontally elongated cross section). The number of coil means the type of shape. Due to the stellarator symmetry, these 20 modular coils consist of 5 different shape coils. The number of coil means the type of shape, namely the same number of coil corresponds to the same type of shape.

Fig.2 Poincare plots of CHS-qa magnetic surfaces. Cross sections at the toroidal angle of 0, 45, 90 degrees are shown. The solid line is the plasma boundary for which the modular coil design is made.

Fig.3 Comparison of rotational transform and magnetic well depth for the configuration obtained from modular coil (result by field tracing) and VMEC calculation.

Fig.4 Spectra of CHS-qa magnetic configuration in Boozer coordinate. a) B_{mn} calculated from VMEC result. b) B_{mn} produced by modular coils in the case that the B_{01} evaluation is not included in the coil geometry optimization process. c) B_{mn} produced by modular coils in the case that the B_{01} evaluation is included. d) Neoclassical diffusion coefficient calculated with the Beidler's expression. The ν^* is the collision frequency normalized by the bounce frequency of toroidal banana orbit.

Fig.5 a) $\mathbf{B} \cdot \mathbf{n} / |B|$ as a function of minimum radius of curvature of coils. (b) $\mathbf{B} \cdot \mathbf{n} / |B|$ as a function of minimum distance between coils.

Fig.6 5 types of modular coils for CHS-qa are shown. The radius of curvature is expressed by different color. Modular coils have rectangular cross section, of which area is 16 cm x 21 cm.

Fig.7 Location of 3 pairs of poloidal coils. All poloidal coils are of circular type. a) a bird's-eye view. b) The poloidal cross section of poloidal field coils. Two modular coils (coil1 and coil5) are also shown at the same poloidal cross section. Auxiliary toroidal field coils are not shown.

Fig.8 Poincare plots when vertical field is applied. a) An inward shift case and b) an outward shift case. The vertical field is 1 % of main magnetic field strength in both cases. Solid line is the plasma boundary for which the modular coil design is made.

Fig.9 Profiles of rotational transform and magnetic well in the magnetic axis control. The amount of vertical field applied is 1 % of main magnetic field strength. In the case of inward shift, rotational transform decreases and magnetic well

becomes deeper.

Fig.10 Spectra of magnetic field strength in Boozer coordinate in the case of magnetic axis shift. a) A case of inward axis shift. b) A case of outward axis shift. Each magnetic configuration is same as shown in Fig.8. c) Neoclassical diffusion coefficient of electron. In the inward shift case, quasi-axisymmetric characteristic is degraded compared with that of the outward shift case.

Fig.11 Magnetic surface when shaping control is applied by quadrupole field. a) deformation of vertical elongation, b) deformation of horizontal elongation. The amount of quadrupole field is 0.75% of main magnetic field strength at (R,Z) = (1.5 m, 0.4 m).

Fig.12 Profiles of rotational transform and magnetic well depth in the case that shaping control by quadrupole field is applied.

Fig.13 Spectra of magnetic field strength in Boozer coordinate in the case that mirror ripple is controlled. By changing the ratio of current in modular coils, the mirror ripple component, B_{01}, can be increased. Except for the second harmonics (B_{02}) of this mirror ripple, differences in other components are small.

Fig.14 Poincare plots in the case that mirror ripple is controlled. Changes in geometry of the outermost magnetic surface are small.

Fig.15 The profiles of rotational transform and magnetic well in the case that mirror ripple is controlled. The standard case is shown as a reference. No significant change can be seen in the magnetic well depth.

Fig.16 The diffusion coefficient of large mirror ripple case of CHS-qa is shown. For the comparison, those of CHS-qa standard configuration and of CHS heliotron/torsatron (Rax=92.1cm) are also shown. No electric field is included. In the evaluation of the diffusion coefficient, the magnetic field model, which is suggested by Beidler and Hitchon, is used.

Fig.17 Rotational transform in the case that an additional toroidal field is applied. The amount of additional toroidal field is +3.2% (or -3.3%) of the main magnetic field strength. A straight dotted line shows the rotational transform of 1/3, where large islands appear.

Fig.18 An example where the size of islands is reduced by coil optimization. a) magnetic surfaces in the case that additional toroidal field is applied. Magnetic islands appear at rational surfaces (ρ = 0.55, and ρ = 0.9). The size of islands is reduced in b) by the coil optimization. The profile of rotational transform is the same for a) and b).

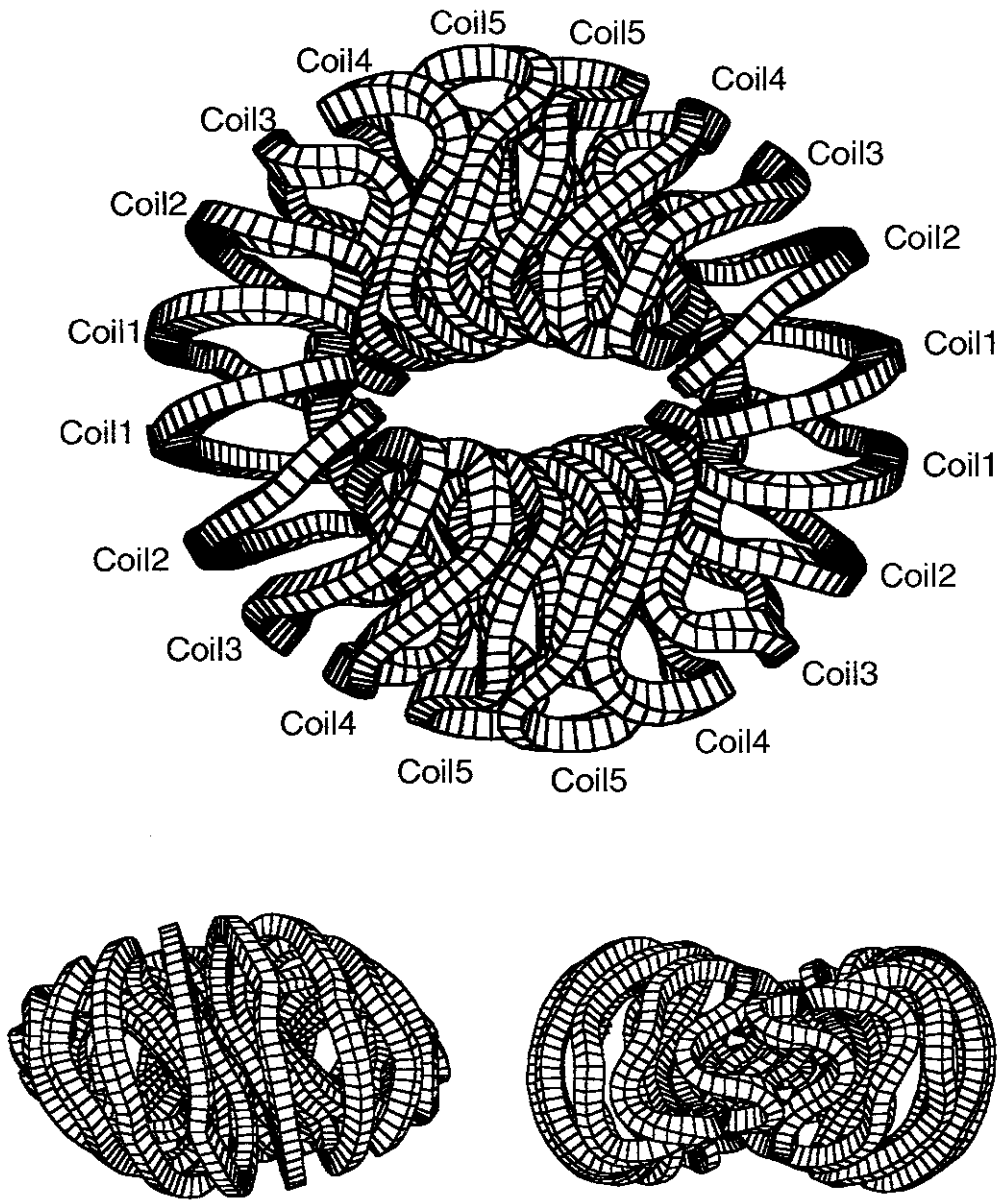
Coil5
Coil5
Coil4
Coil4
Coil3
Coil3
Coil2
Coil2
Coil1
Coil1
Coil1
Coil1
Coil2
Coil2
Coil3
Coil3
Coil4
Coil4
Coil5
Coil5

Fig.1

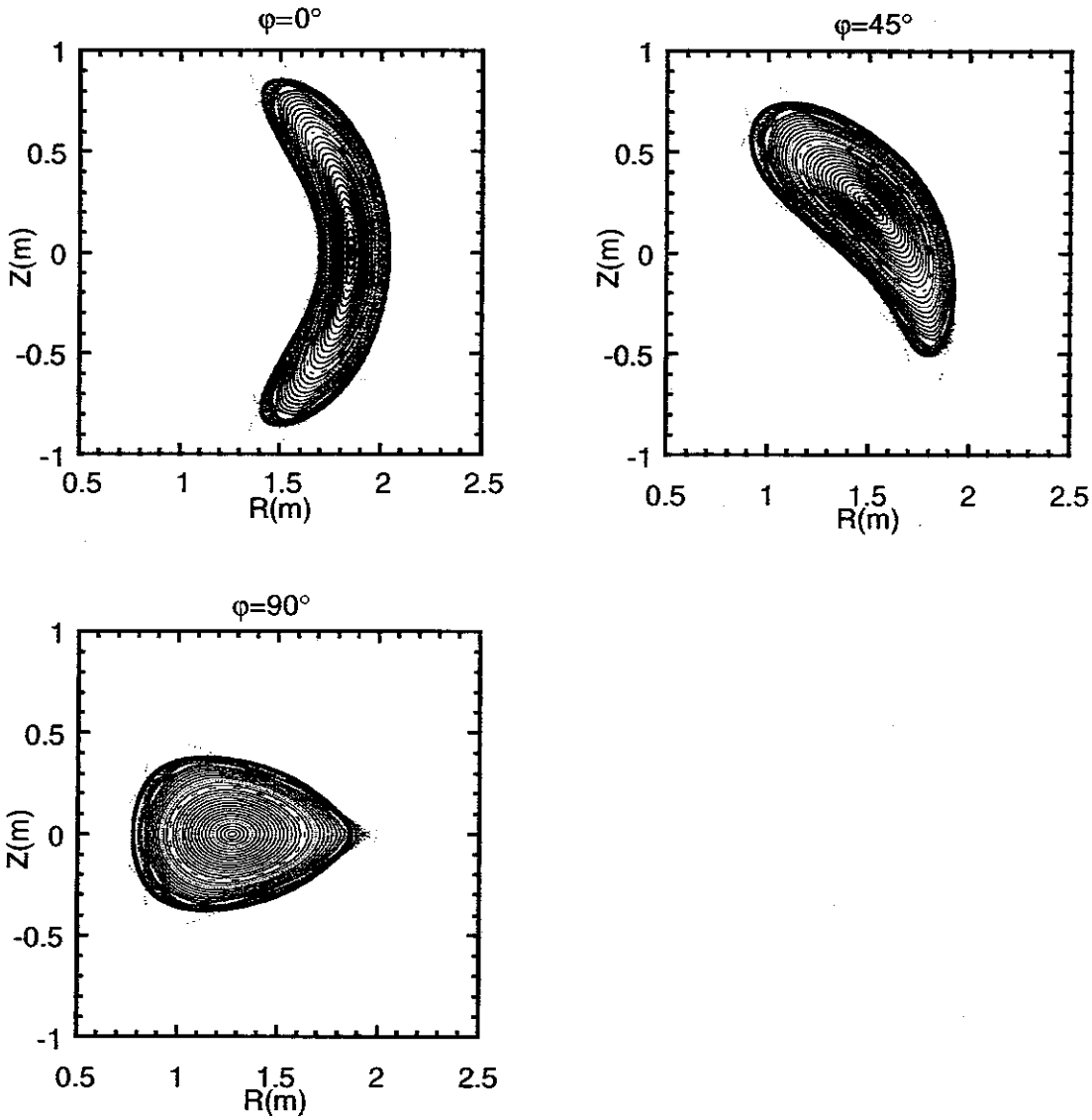

Fig.2

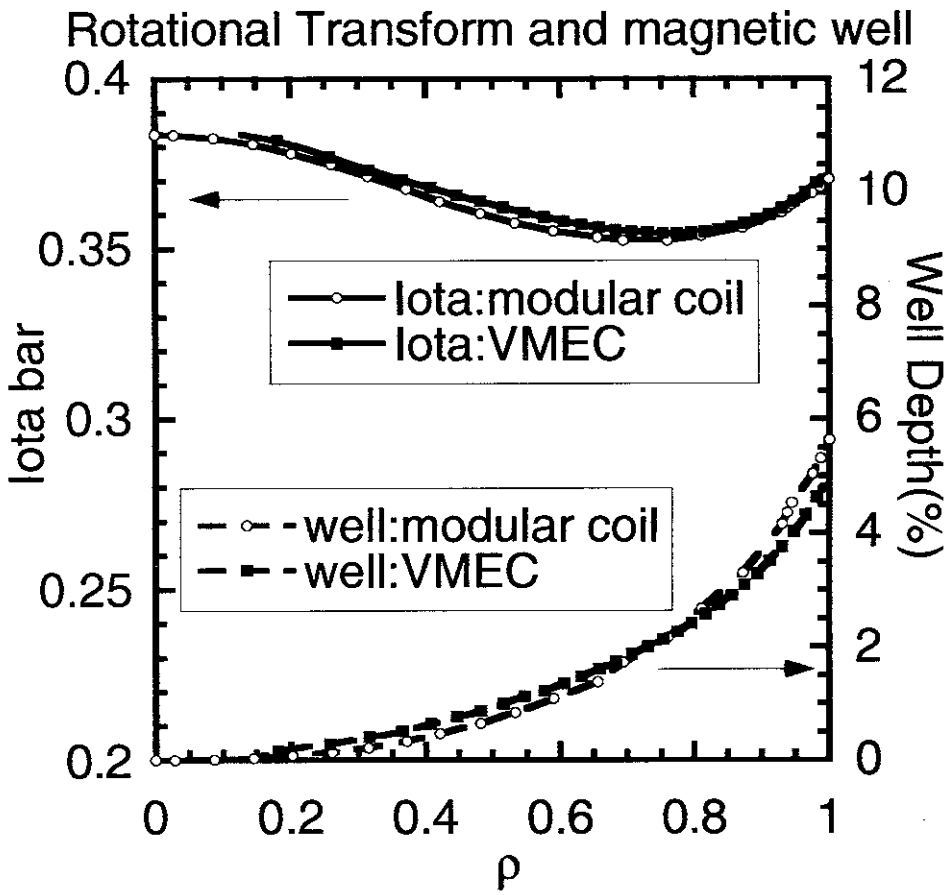
Rotational Transform and magnetic well
0.4
0.35
0.3
0.25
0.2
Iota bar
12
10
8
6
4
2
0
Well Depth(%)
Iota:modular coil
Iota:VMEC
well:modular coil
well:VMEC
0
0.2
0.4
0.6
0.8
1
ρ

Fig.3

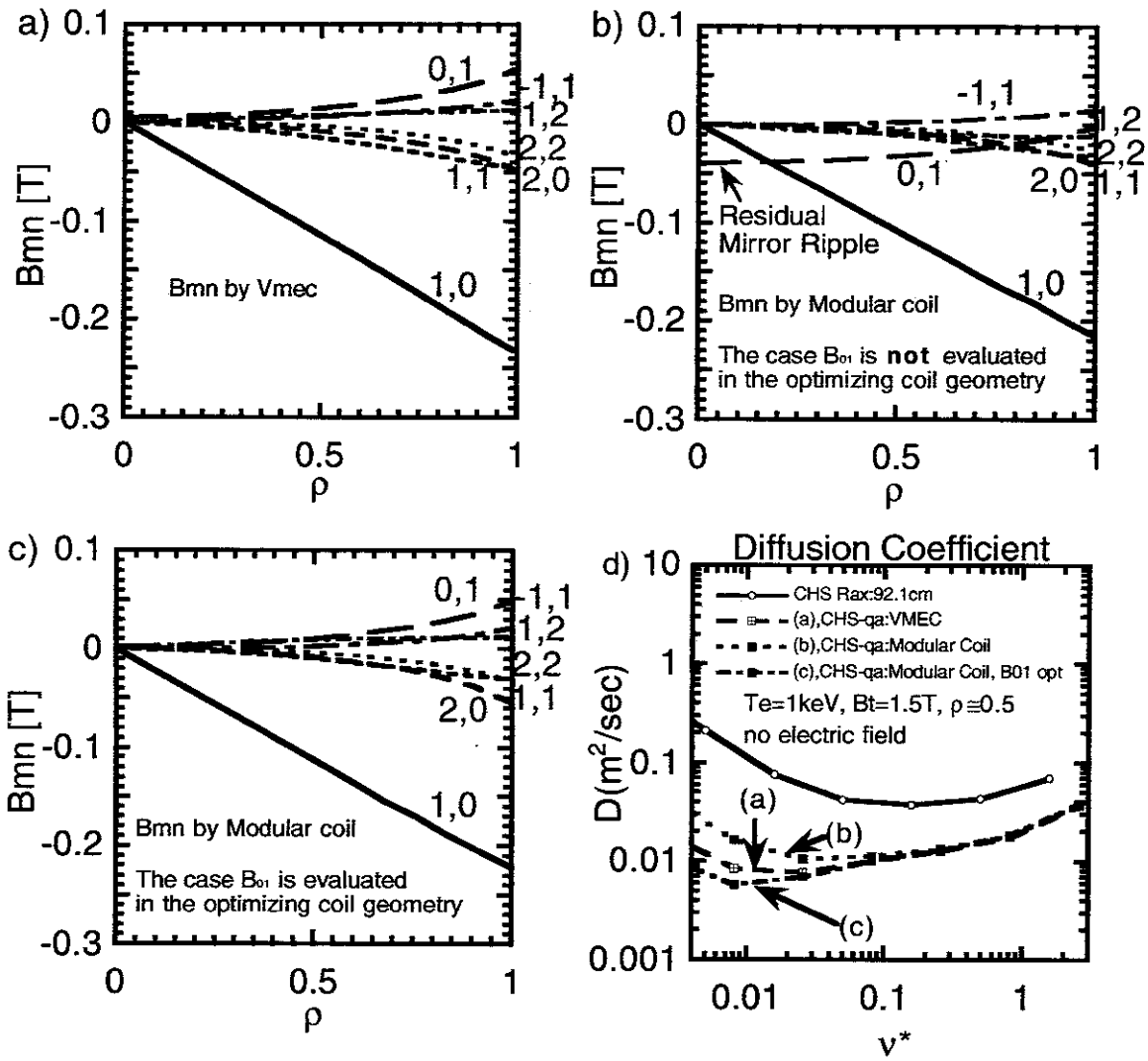
a) 0.1
0
-0.1
-0.2
-0.3
Bmn [T]
0
0.5
1
ρ
0,1
-1,1
1,2
2,2
1,1
2,0
1,0
Bmn by Vmec
b) 0.1
Residual
Mirror Ripple
Bmn by Modular coil
The case B01 is not evaluated
in the optimizing coil geometry
c) 0.1
Bmn by Modular coil
The case B01 is evaluated
in the optimizing coil geometry
d) 10
Diffusion Coefficient
CHS Rax:92.1cm
(a),CHS-qa:VMEC
(b),CHS-qa:Modular Coil
(c),CHS-qa:Modular Coil, B01 opt
Te=1keV, Bt=1.5T, ρ≅0.5
no electric field
D(m²/sec)
1
0.1
0.01
0.001
0.01
0.1
1
ν*
(a)
(b)
(c)

Fig.4

a)

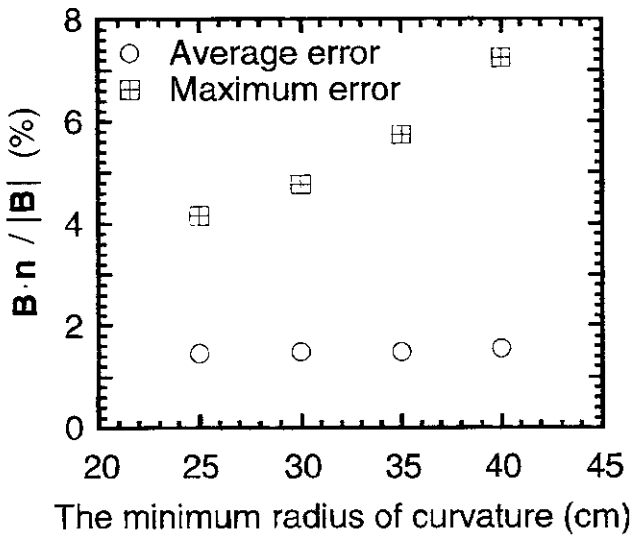
Average error
Maximum error
B·n / |B| (%)
0
2
4
6
8
20
25
30
35
40
45
The minimum radius of curvature (cm)

b)

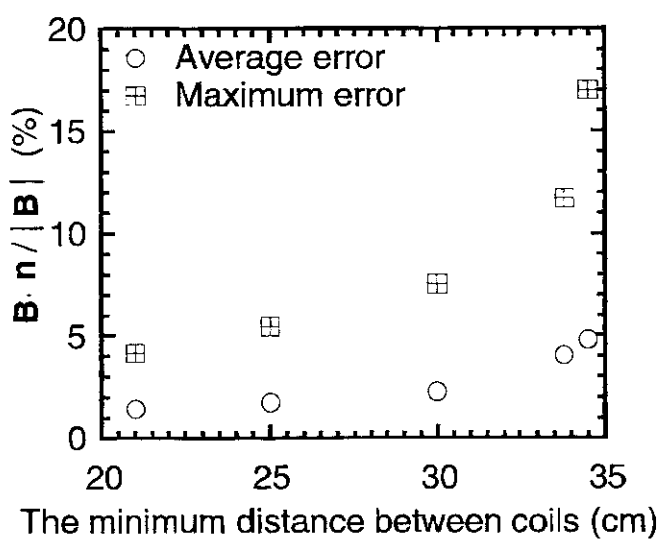
Average error
Maximum error
B·n / |B| (%)
0
5
10
15
20
20
25
30
35
The minimum distance between coils (cm)

Fig.5

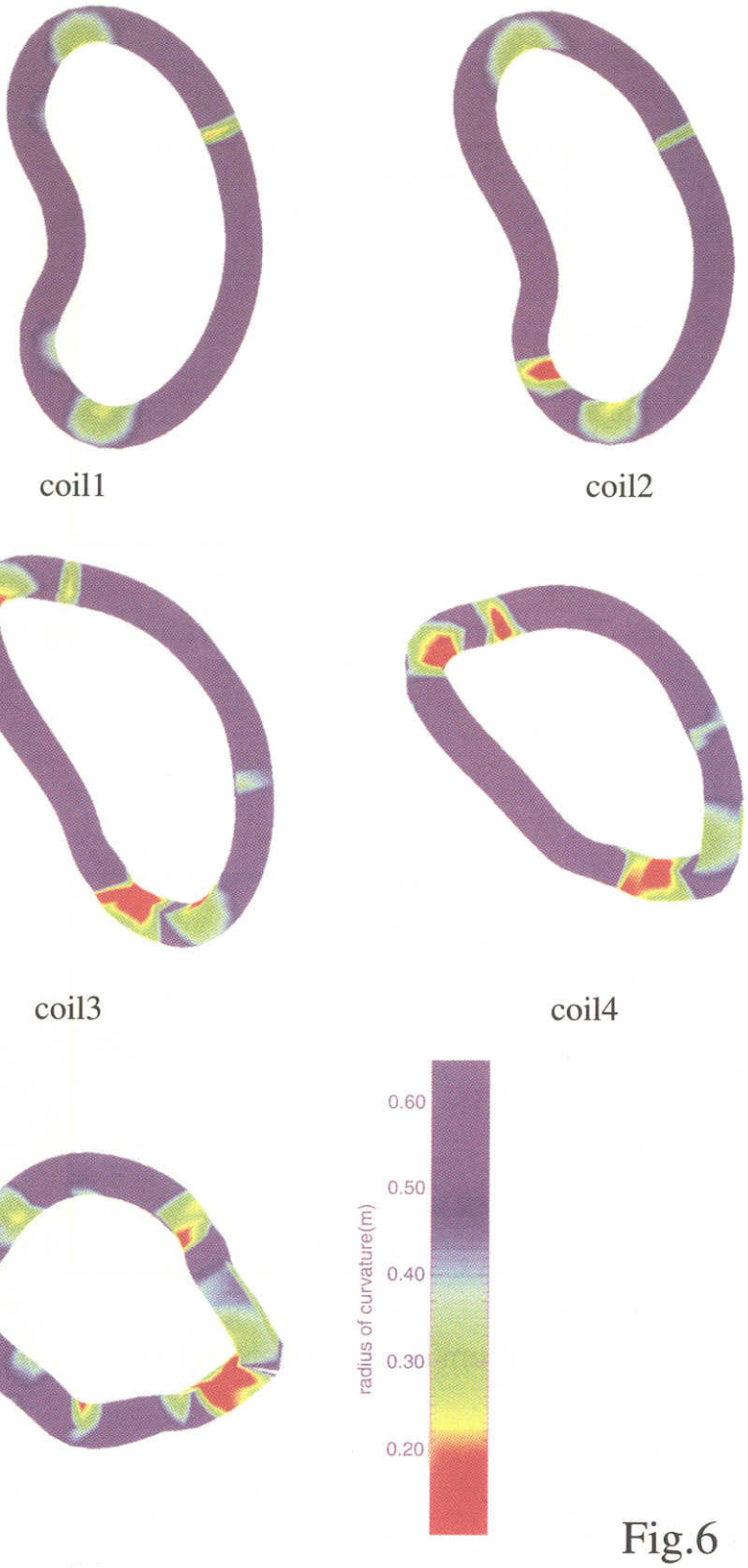
coil1
coil2
coil3
coil4
coil5
0.60
0.50
0.40
0.30
0.20
radius of curvature(m)

Fig.6

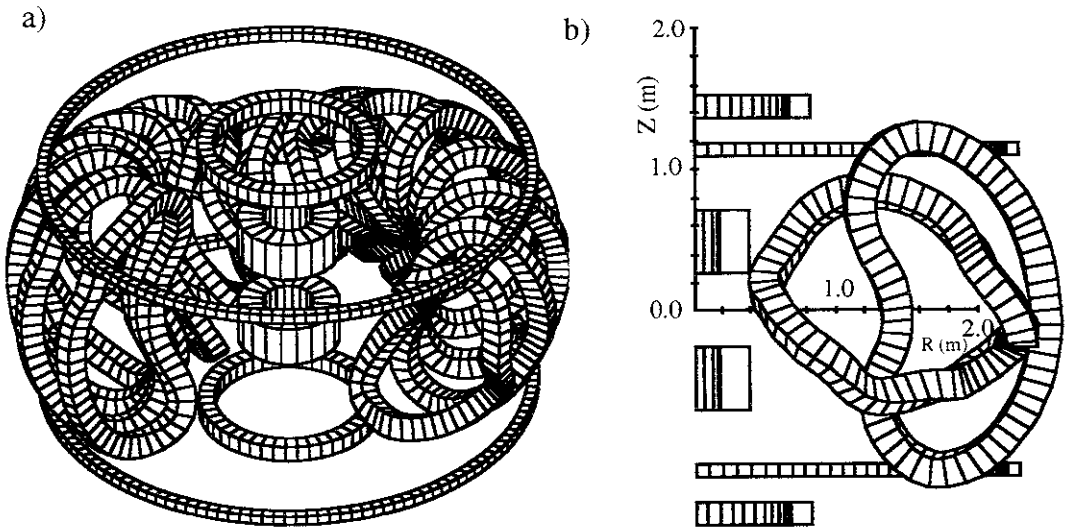
a)
b)
2.0
Z (m)
1.0
0.0
1.0
2.0
R (m)

Fig.7

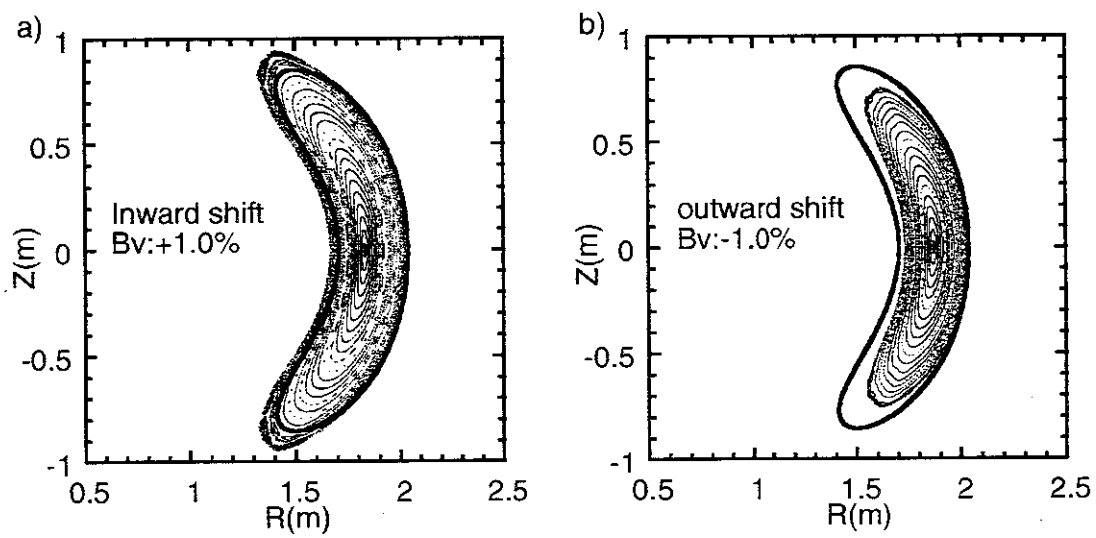
a)
Inward shift
Bv:+1.0%
Z(m)
R(m)
b)
outward shift
Bv:-1.0%
Z(m)
R(m)

Fig.8

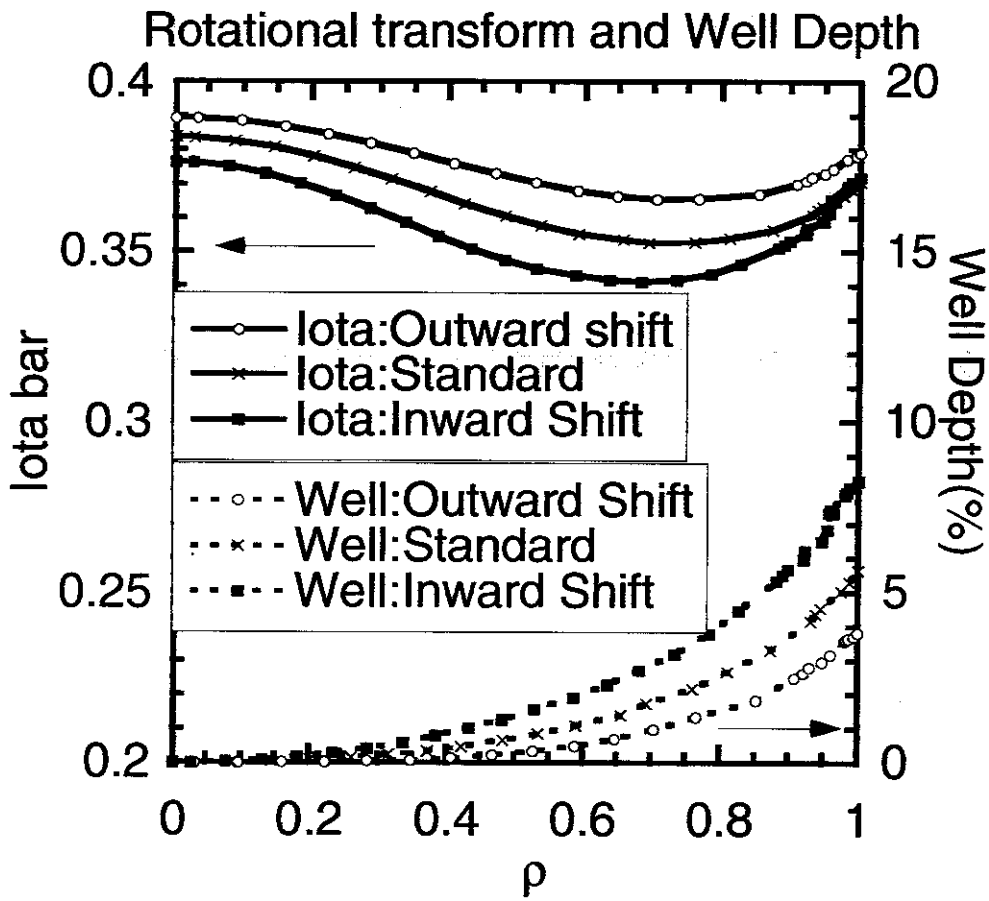
Rotational transform and Well Depth
0.4
0.35
0.3
0.25
0.2
Iota bar
20
15
10
5
0
Well Depth(%)
Iota:Outward shift
Iota:Standard
Iota:Inward Shift
Well:Outward Shift
Well:Standard
Well:Inward Shift
0
0.2
0.4
0.6
0.8
1
ρ

Fig.9

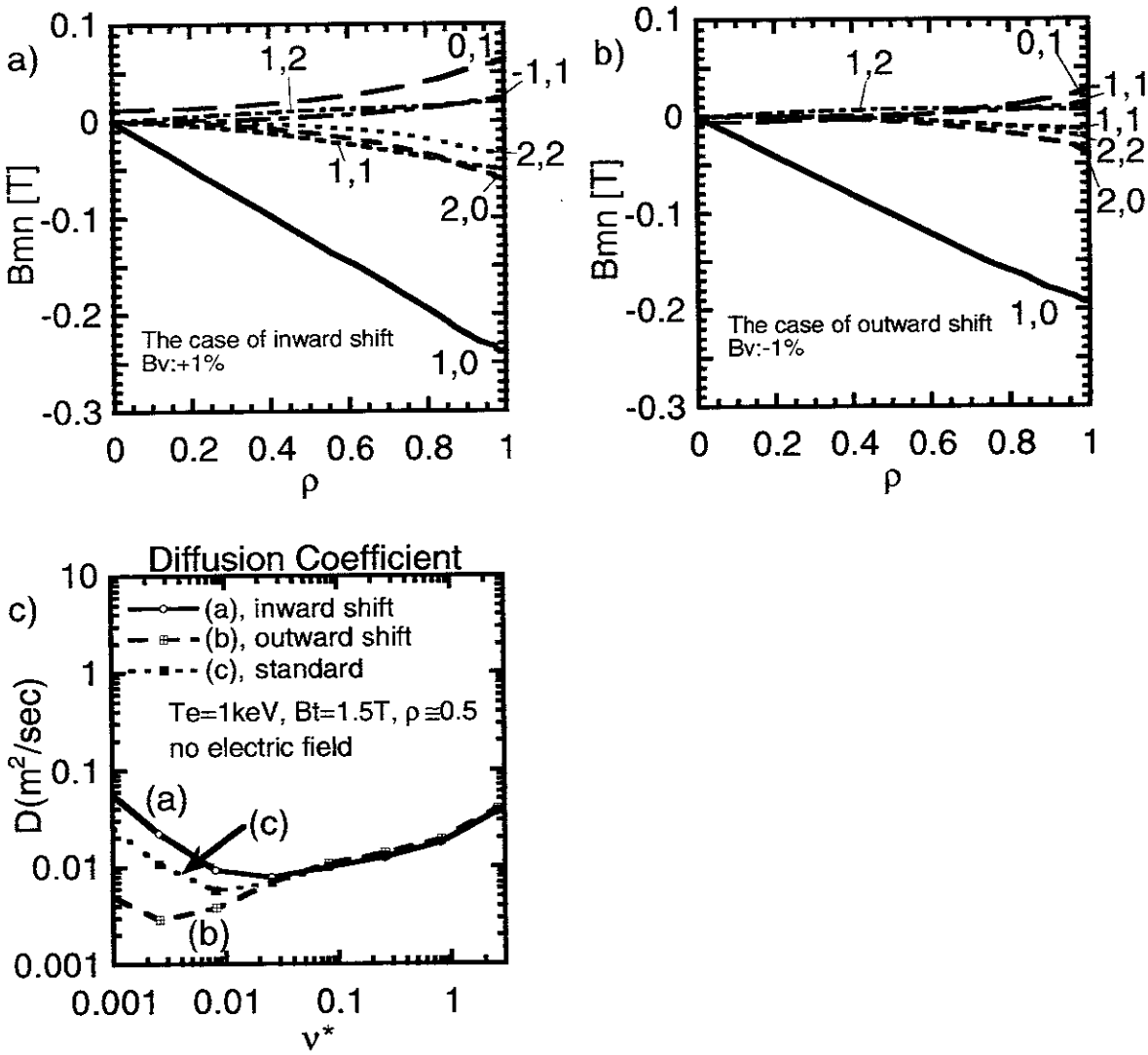
a)
b)
c)
Bmn [T]
ρ
1,2
0,1
-1,1
1,1
2,2
2,0
1,0
The case of inward shift
Bv:+1%
The case of outward shift
Bv:-1%
Diffusion Coefficient
(a), inward shift
(b), outward shift
(c), standard
Te=1keV, Bt=1.5T, ρ≡0.5
no electric field
D(m²/sec)
ν*

Fig.10

a)

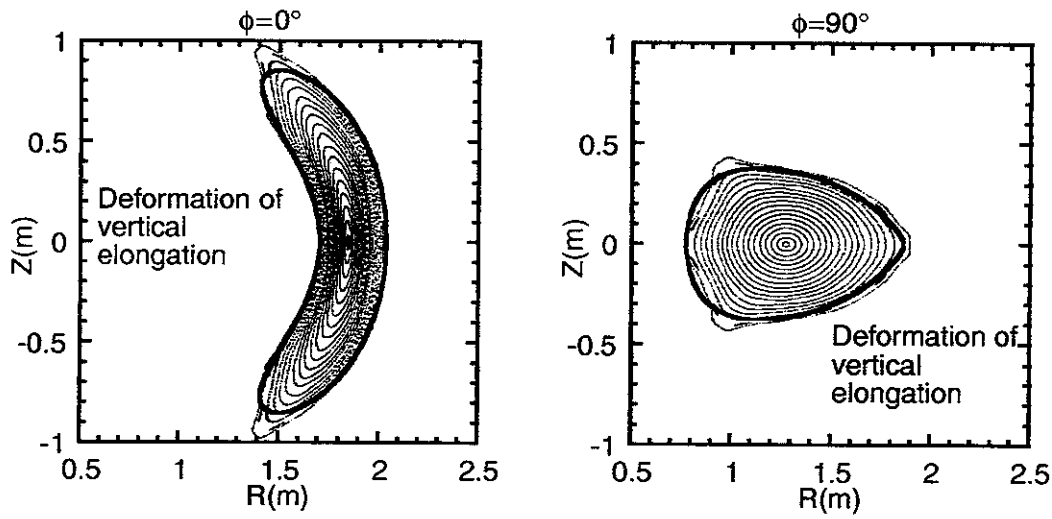
ϕ=0°
Deformation of vertical elongation
Z(m)
R(m)
ϕ=90°
Deformation of vertical elongation
Z(m)
R(m)

b)

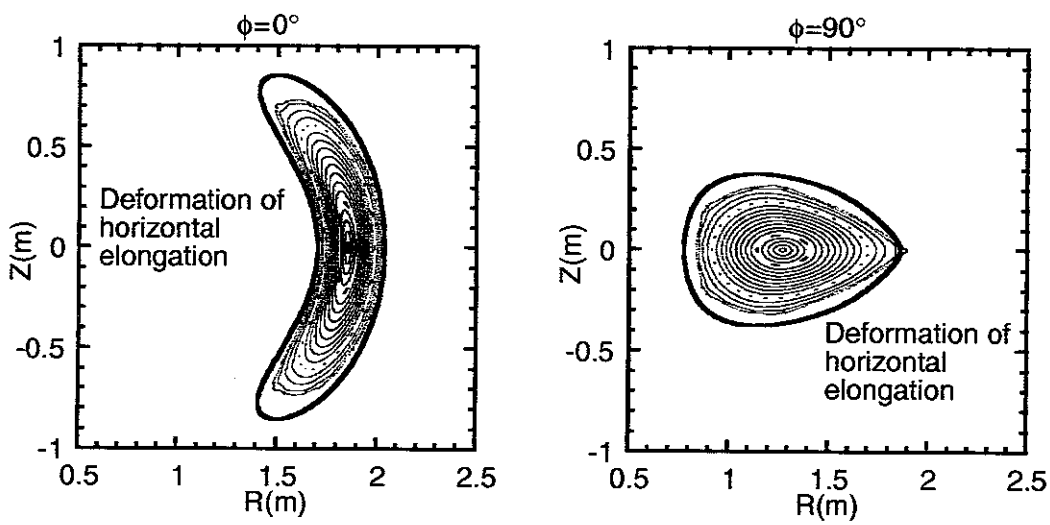
ϕ=0°
Deformation of horizontal elongation
Z(m)
R(m)
ϕ=90°
Deformation of horizontal elongation
Z(m)
R(m)

Fig.11

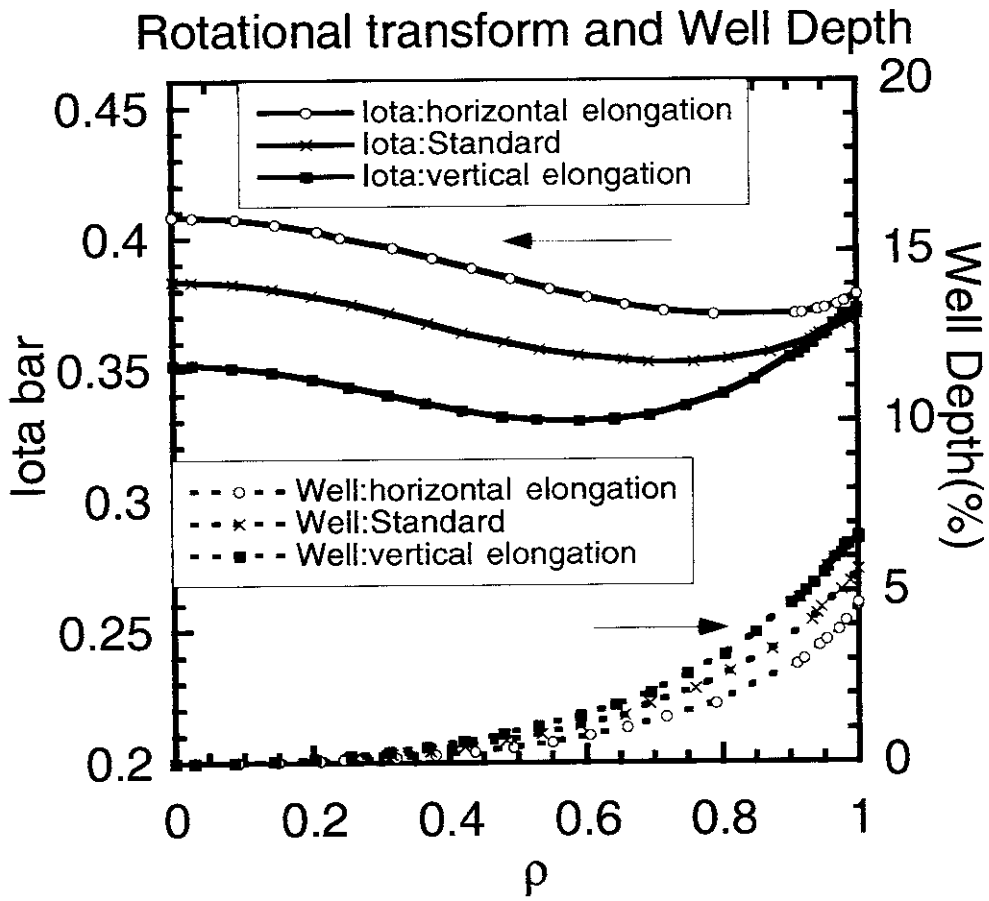
Rotational transform and Well Depth
Iota:horizontal elongation
Iota:Standard
Iota:vertical elongation
Well:horizontal elongation
Well:Standard
Well:vertical elongation
Iota bar
Well Depth(%)
ρ
0.45
0.4
0.35
0.3
0.25
0.2
20
15
10
5
0
0
0.2
0.4
0.6
0.8
1

Fig.12

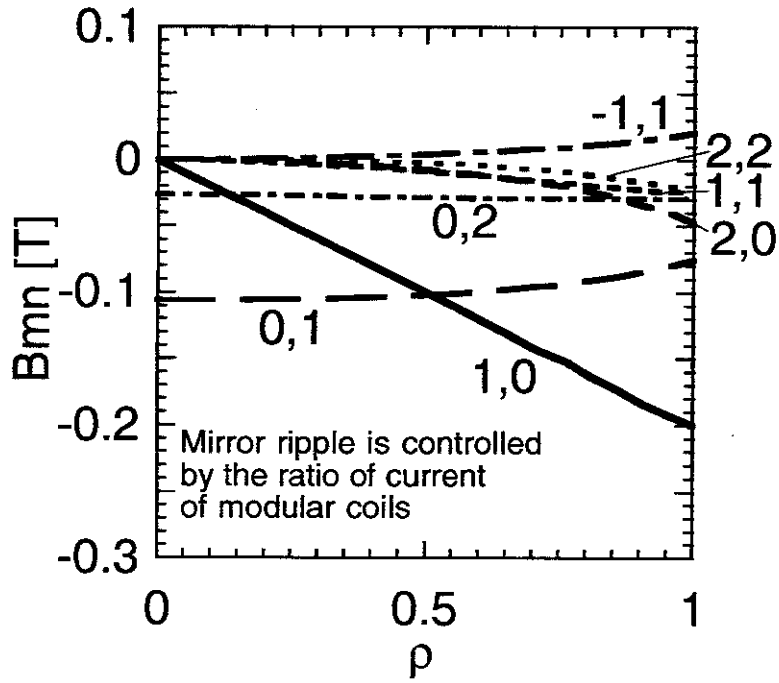
0.1
0
-0.1
-0.2
-0.3
Bmn [T]
0
0.5
1
ρ
-1,1
2,2
1,1
2,0
0,2
0,1
1,0
Mirror ripple is controlled
by the ratio of current
of modular coils

Fig.13

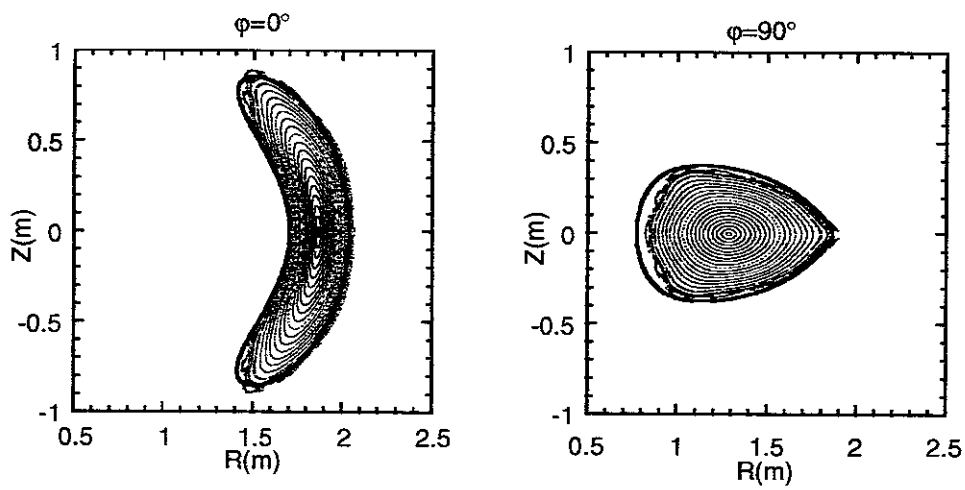
φ=0°
φ=90°
Z(m)
R(m)
1
0.5
0
-0.5
-1
0.5
1
1.5
2
2.5

Fig.14

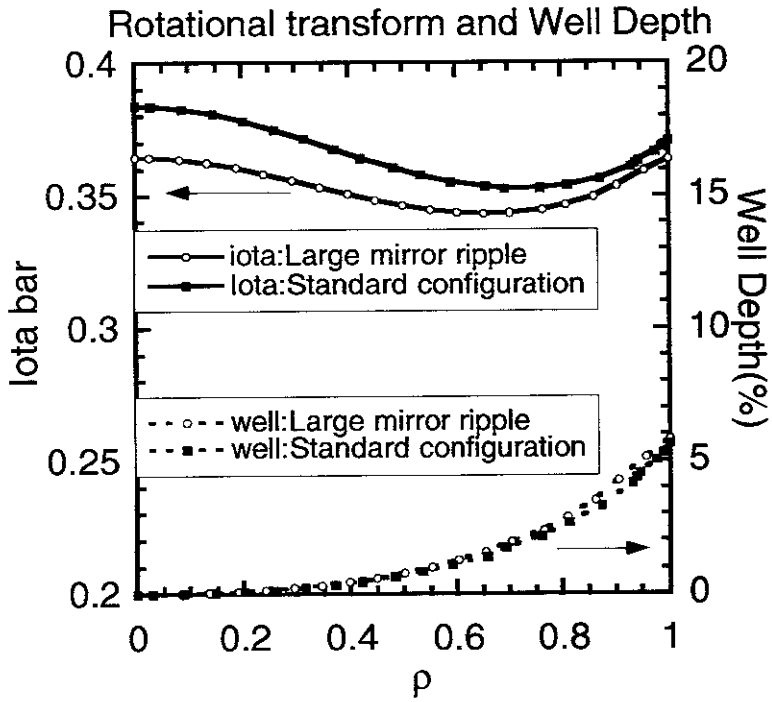
Rotational transform and Well Depth
0.4
0.35
0.3
0.25
0.2
Iota bar
20
15
10
5
0
Well Depth(%)
iota:Large mirror ripple
Iota:Standard configuration
well:Large mirror ripple
well:Standard configuration
0
0.2
0.4
0.6
0.8
1
ρ

Fig.15

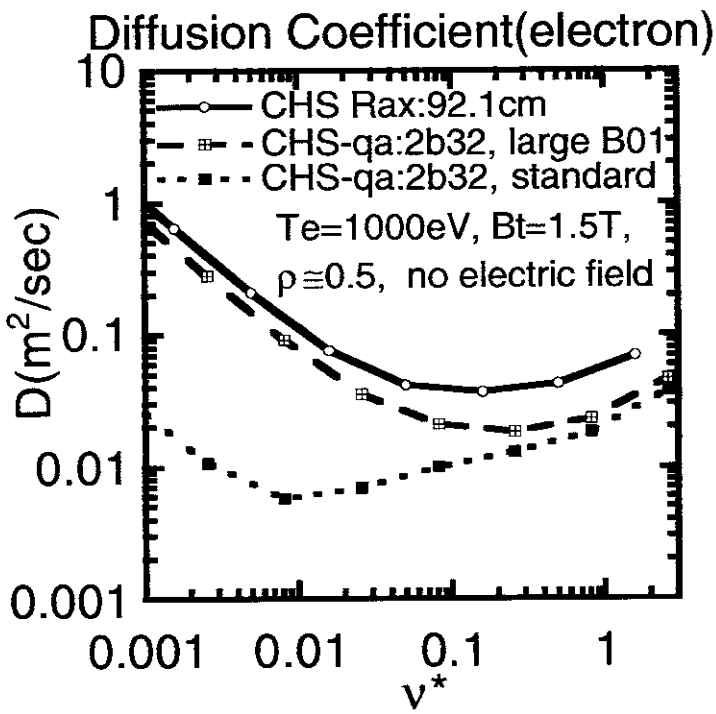
Diffusion Coefficient(electron)
10
1
0.1
0.01
0.001
D(m²/sec)
CHS Rax:92.1cm
CHS-qa:2b32, large B01
CHS-qa:2b32, standard
Te=1000eV, Bt=1.5T,
ρ≅0.5, no electric field
0.001
0.01
0.1
1
ν*

Fig.16

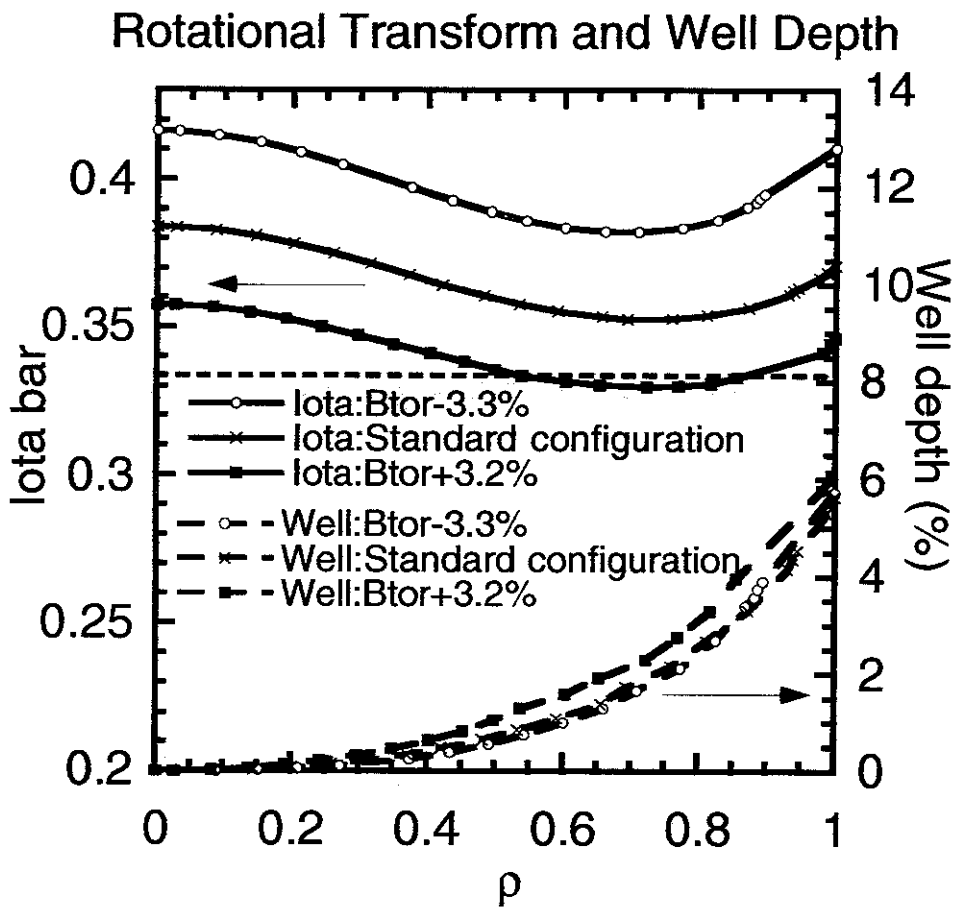
Rotational Transform and Well Depth
Iota bar
Well depth (%)
ρ
0.4
0.35
0.3
0.25
0.2
14
12
10
8
6
4
2
0
0
0.2
0.4
0.6
0.8
1
Iota:Btor-3.3%
Iota:Standard configuration
Iota:Btor+3.2%
Well:Btor-3.3%
Well:Standard configuration
Well:Btor+3.2%

Fig.17

a)

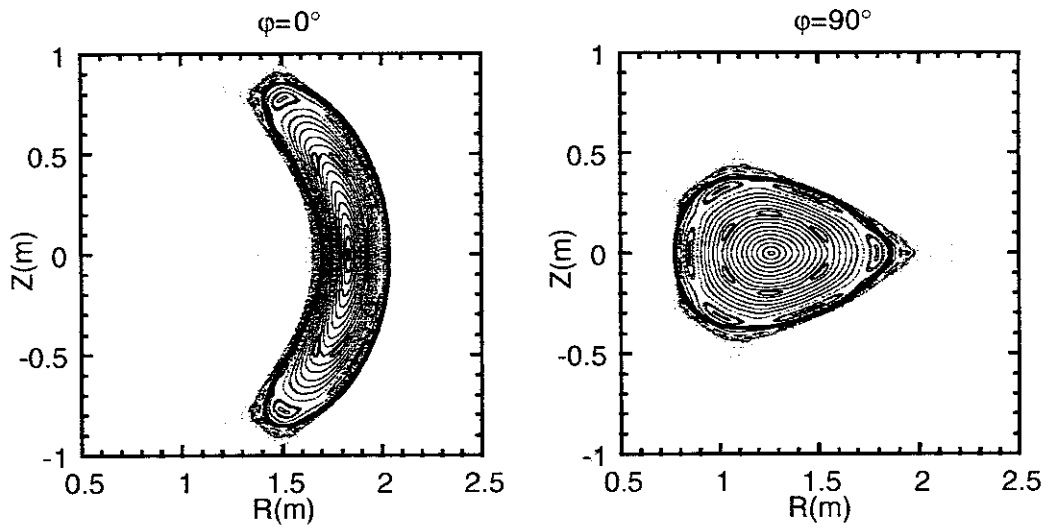

b)

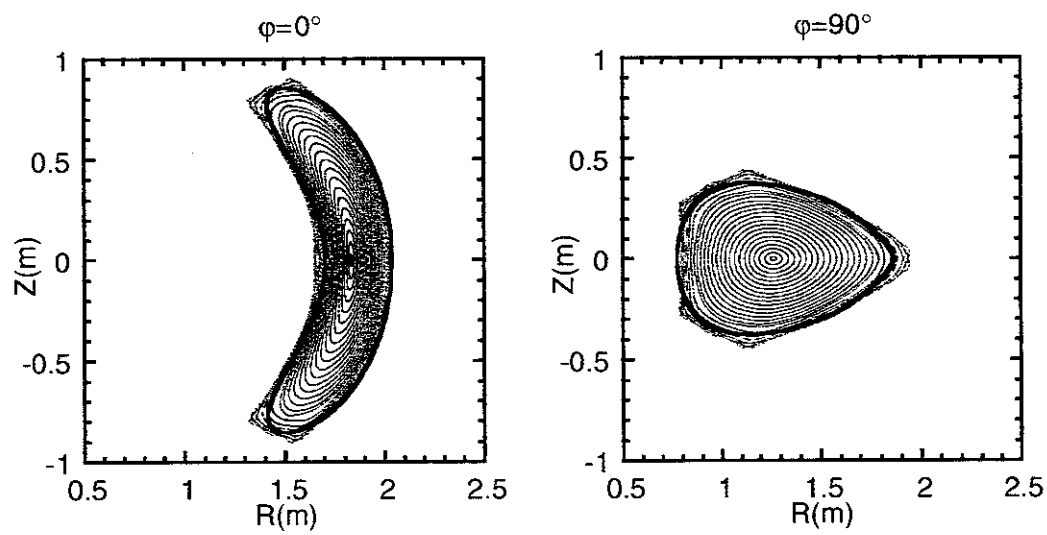

Fig.18